FISSION REACTORS

KEYWORDS: *space propulsion, neutronic/thermal-hydraulic coupling, particle bed reactor*

# ASSESSMENT OF THE IMPACT OF NEUTRONIC/THERMAL-HYDRAULIC COUPLING ON THE DESIGN AND PERFORMANCE OF NUCLEAR REACTORS FOR SPACE PROPULSION

SHASHIKANT M. AITHAL, TUNC ALDEMIR, and KAMBIZ VAFAI
*The Ohio State University, Department of Mechanical Engineering*
*Nuclear Engineering Program, 206 West Eighteenth Avenue, Columbus, Ohio 43210*

Received May 12, 1993
Accepted for Publication September 21, 1993

*A series of studies has been performed to investigate the potential impact of the coupling between neutronics and thermal hydraulics on the design and performance assessment of solid core reactors for nuclear thermal space propulsion, using the particle bed reactor (PBR) concept as an example system. For a given temperature distribution in the reactor, the $k_{eff}$ and steady-state core power distribution are obtained from three-dimensional, continuous energy Monte Carlo simulations using the MCNP code. For a given core power distribution, determination of the temperature distribution in the core and hydrogen-filled annulus between the reflector and pressure vessel is based on a nonthermal equilibrium analysis. The results show that a realistic estimation of fuel, core size, and control requirements for PBRs using hydrogenous moderators, as well as optimization of the overall engine design, may require coupled neutronic/thermal-hydraulic studies. However, it may be possible to estimate the thermal safety margins and propellant exit temperatures based on power distributions obtained from neutronic calculations at room temperature. The results also show that, while variation of the hydrogen flow rate in the annulus has been proposed as a partial control mechanism for PBRs, such a control mechanism may not be feasible for PBRs with high moderator-to-fuel ratios and hence soft core neutron spectra.*

## I. INTRODUCTION

Efforts to utilize nuclear power for space propulsion began when the ROVER/NERVA program was set up in 1956. Between 1956 and 1973, several experimental reactors and ground engines were developed, such as the Kiwi, NRX, Phoebus, and XE series. Although the program was successful and the Phoebus 2A reactor was operated[1] on June 1968 at a power level of 4100 MW(thermal) for 12 min, the program was terminated in 1973 due to perceived lack of mission.

Reexamination of the nuclear option for space propulsion started in the early 1980s as part of the SP-100 program.[2] Several reactor concepts have been proposed for nuclear thermal propulsion (NTP) and nuclear electric propulsion (NEP) since then.[3-9] These concepts cover a wide spectrum, ranging from the previously tested solid core concepts[9] to systems that may pose major technological challenges (e.g., gaseous cores[5]). The reference list only provides examples and is not intended to be exhaustive. In NTP, the propellant/coolant (i.e., hydrogen) picks up heat directly from the reactor and exits through a converging-diverging nozzle providing thrust. In the previously tested NTP concepts, the propellant passes through an annulus between the reflector and pressure vessel before entering the core (Fig. 1) to cool the reflector and also to improve the thermodynamic efficiency of operation. In NEP, the nuclear reactor is used as a heat-generating source to produce electricity by means of thermionic or thermoelectric converters.

Following the commencement of the Space Exploration Initiative in 1989 directed at establishing permanent human presence beyond earth orbit, the National Aeronautics and Space Administration (NASA) began performing studies for a number of mission scenarios to identify the key technologies needed to bring these missions to realization. The studies have shown that nuclear propulsion can lead to substantial mass savings and subsequently savings on mission times,[10] and the findings of a series of recent NASA U.S. Department of Energy (DOE)/U.S. Department of Defense (DOD) technical panels[11] indicate that NTP using solid cores

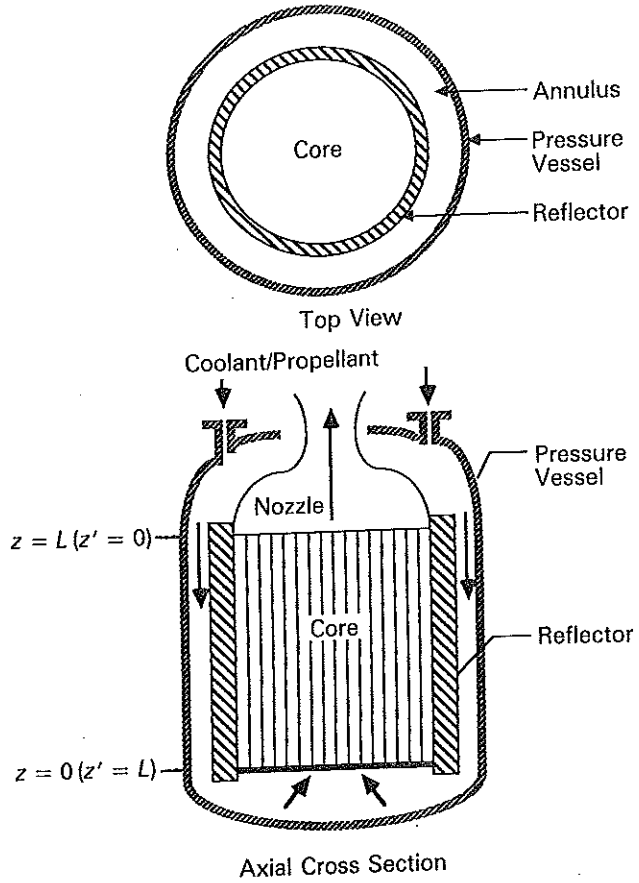


Fig. 1. A reactor concept for NTP applications.

will be the option for the near-term applications by the 2020s. In terms of the fuel utilized, the reactor types under consideration are (a) NERVA and prismatic cermet concepts,[12,13] (b) reactors using particle fuel,[14,15] and (c) reactors using refractory fuel.[16] The first two groups of reactors are thermal reactors and the third group of reactors is fast reactors.

Irrespective of the reactor type used, the axial temperature gradient in the core is expected to be very large (~50 K/cm), since all the proposed engine concepts have small cores (~60 cm high, 50 to 80 cm in diameter) and propellant exit temperatures of ~2000 to 2500 K. Even for thermal reactor cores that would be using highly enriched uranium fuels to reduce core size and weight and hence may have negligible temperature feedback due to the Doppler broadening of $^{238}U$ resonances, such a large temperature gradient will cause substantial local shifting in the thermal neutron spectrum with possible subsequent changes in the neutron-nuclei reaction rates. Two recent studies[17,18] have also shown that (a) the neutrons reflected back to the core from the pressure vessel may contribute significantly to the neutron economy and (b) there may be tight space-energy-temperature coupling between the reflector, hydrogen in the annulus, and the pressure vessel.

Although the need for coupled neutronic/thermal-hydraulic analyses in the design and performance assessment of the reactors for space propulsion has been anticipated and software development to reduce the manual effort in such analyses is under way,[19-21] no studies have been encountered in the available literature that attempt to quantify the potential impact of neutronic/thermal-hydraulic coupling on the predicted reactor characteristics under operational conditions. This study uses the particle bed reactor (PBR) concept[3,15] proposed by Brookhaven National Laboratory as an example of a solid core, thermal reactor for NTP to investigate the change in clean core $k_{eff}$, steady-state power, and temperature distributions with the change in the following:

1. the core thermal neutron spectrum due to the increased thermal motion of the medium nuclei under power (core analysis)
2. the fraction of neutrons reflected back to the core due to a change in the heat transfer into the annulus and/or convective heat transfer within the annulus (reflector analysis).

The PBR has been identified as one of the four near-term options for space propulsion by the NASA/DOE/DOD panels.[22] Transient, burnup, and thermal expansion effects are not considered in this study, since the modeling of these effects requires a clearer definition of the system and hence the mission requirements.[11] However, it should be noted that several pertinent aspects of the transient and startup effects with respect to the thermal-hydraulic part of the problem have been analyzed in Ref. 23. Reflector analysis (i.e., item 2 in the preceding list) is also relevant to the controllability of the reactor by varying the hydrogen flow rate in the annulus. Reference 17 shows that a 400 K temperature increase in the hydrogen flowing through the annulus can reduce the $k_{eff}$ by ~3% $\Delta k/k$ in a beryllium moderated and reflected PBR. However, it is not clear that this behavior can be generalized to other core configurations. Section II describes the PBR under consideration in this study. Computational modeling of the system and the analyses are described in Secs. III and IV, respectively. The conclusions of the study are given in Sec. V.

## II. SYSTEM DESCRIPTION

The PBR uses fuel in the form of small-diameter particles (100 to 500 $\mu$m), which consist of a highly enriched uranium kernel surrounded by multiple layers of pyrographite and sometimes additional zirconium carbide (ZrC) or silicon carbide layers (Fig. 2). The fuel particles are held between the two porous annuli ("frits") to form a fuel element (Fig. 3), and the fuel elements are embedded in the moderator block in concentric rings to form the core (Fig. 4). The moderator block

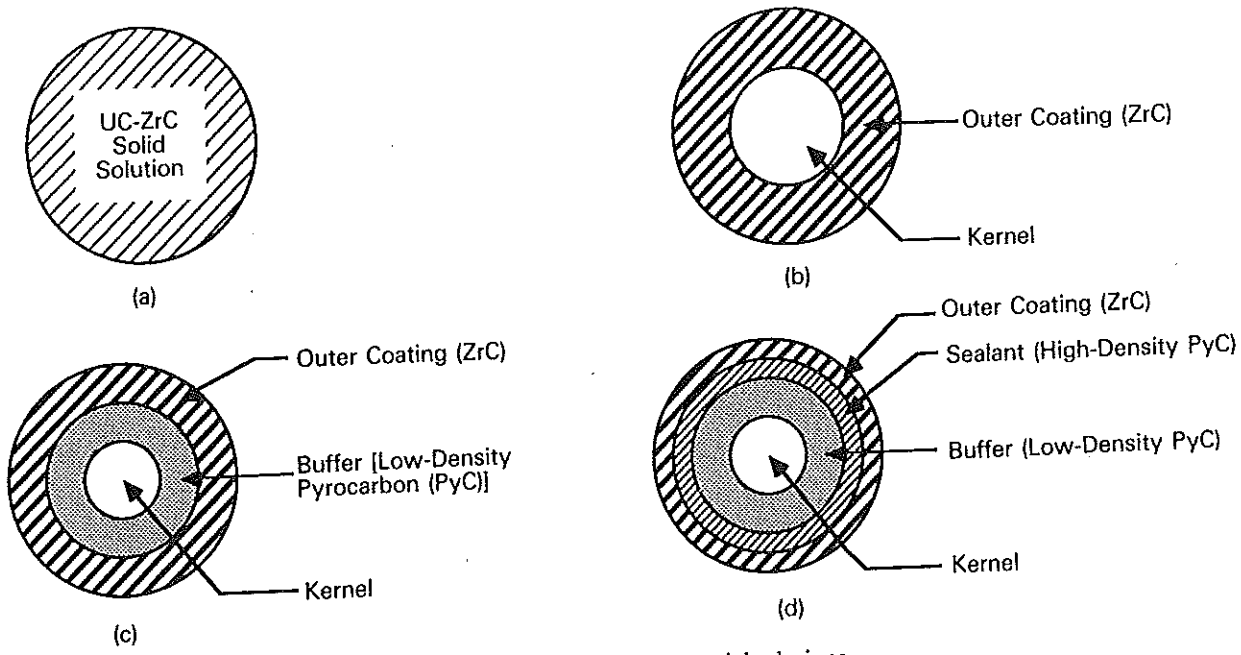


Fig. 2. Several PBR fuel particle designs.

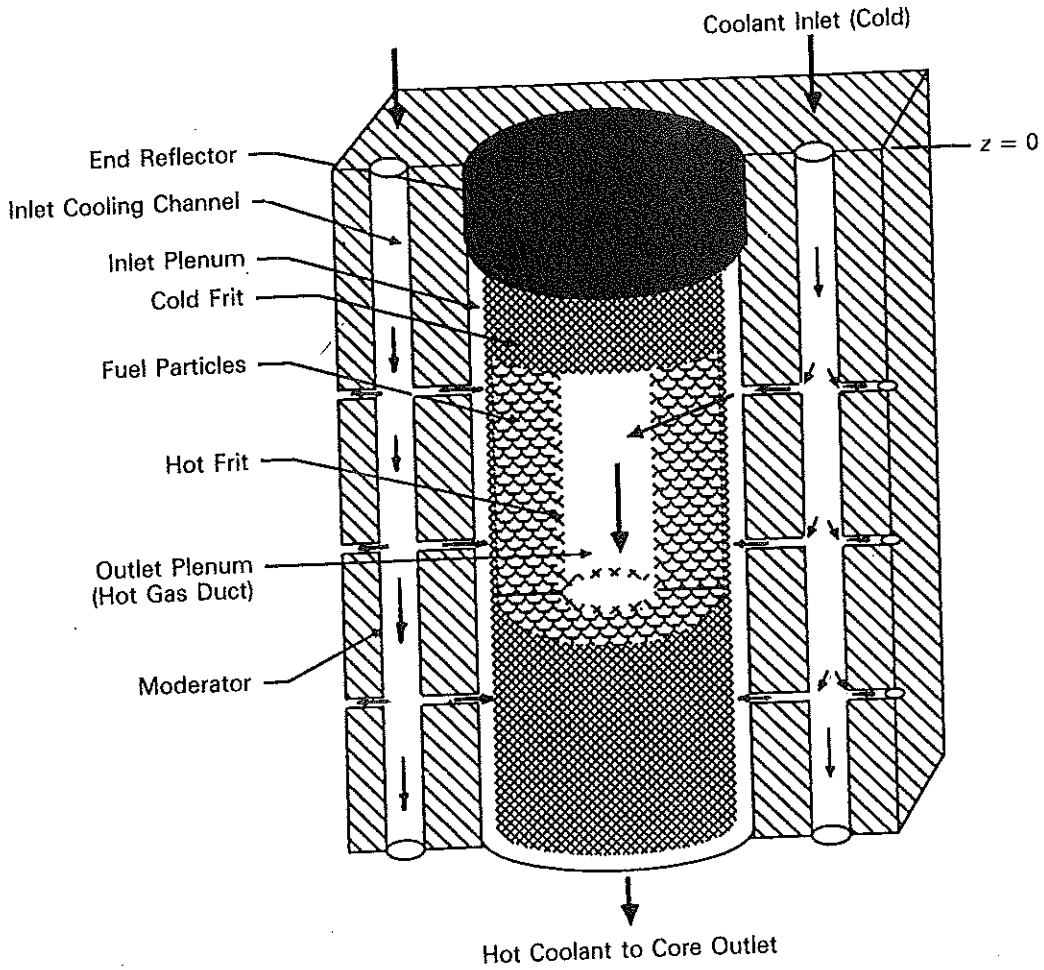


Fig. 3. Axial view of a PBR fuel element. Arrows indicate the path of the coolant flow through the coolant channels and the fuel element.

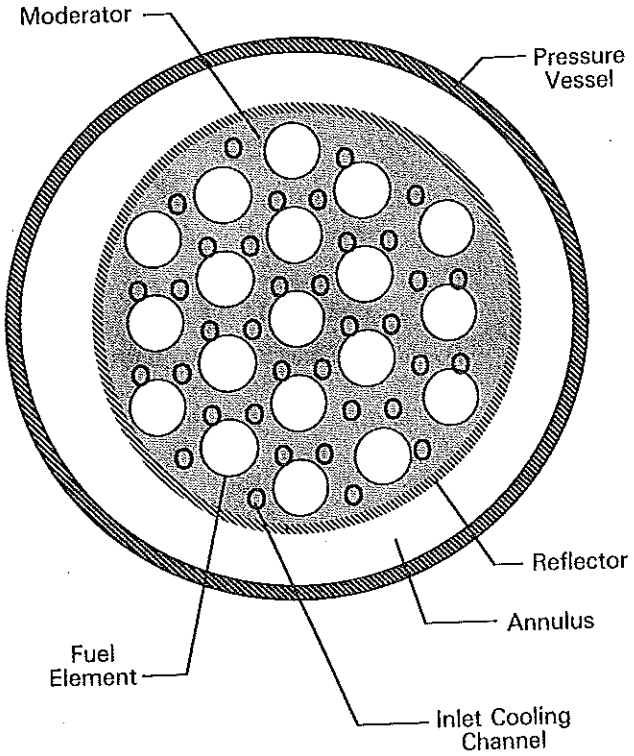


Fig. 4. PBR core.

is surrounded by a pressure vessel, reflected radially and axially for neutron economy. Hydrogen pumped from the propellant tank flows through an annulus located between the radial reflector and the pressure vessel before entering the core (see Fig. 1). After entering the core, the coolant first passes through the outer cold frit (see Fig. 3), then directly over the fuel particles and finally through the inner hot frit into the outlet plenum to be ejected through a nozzle to develop thrust. Partial reactivity control is achieved by varying the hydrogen mass flow rate in the annulus (see Figs. 1 and 4). Tables I and II list the PBR component materials and dimensions, respectively, considered in this study. The main advantages[24] of PBRs are

TABLE I

PBR Component Materials Under Consideration

| Component | Material |
|---|---|
| Moderator | Be, $ZrH_{1.7}$ |
| Cold frit | Zircaloy-2 |
| Hot frit | ZrC |
| Fuel particles | UC kernel, ZrC coating |
| Pressure vessel | Stainless steel |
| End reflectors | Graphite |
| Radial reflector | Beryllium |

TABLE II

PBR Dimensions Used in the Study

| | |
|---|---|
| Core radius (cm) | 22.5 (19 elements) |
| Core height (cm) | 60 |
| Pressure vessel thickness (cm) | 5 |
| End reflector thickness (cm) | 5 |
| Fuel particle diameter (cm) | 0.05 |
| Fuel enrichment (wt% $^{235}U$) | 93.5 |
| Outer plenum diameter (cm) | 2.8 |
| Hot frit thickness (cm) | 0.1 |
| Cold frit thickness (cm) | 0.15 |
| Core lattice pitch (cm) | 8 |
| Inlet coolant channel radius (cm) | 0.66 (36 channels) |
| Inlet plenum thickness (cm) | 0.25 |

1. large heat transfer area and relatively small temperature difference between the fuel and the coolant (which increases the reactor output under given temperature constraints on the materials used)
2. no thermal shock to fuel
3. rapid ascent capability to full power
4. 99.99% retention of fission products
5. available or adaptable fuel.

The PBRs can be used for both NTP and NEP. The PBRs can also be used to obtain on-board electric power.

## III. SYSTEM MODELING

The coupled neutronic/thermal-hydraulic analyses were performed by using sequentially

1. the core power distribution obtained from the neutronic calculations for the determination of temperature distributions in the core and annulus
2. the temperature distributions obtained from the thermal-hydraulic studies for the determination of $k_{eff}$ and core power distribution

until the $k_{eff}$ and core power distributions obtained from two consecutive sets of calculations agreed within specified margins (outer iterations). Sections III.A and III.B describe the neutronic and thermal-hydraulic models used for this purpose, respectively. While another iterative loop would be needed to keep $k_{eff}$ within a target range by adjusting the core size and fuel enrichment, consideration of such a loop is outside the scope of this paper, whose objectives are to study the impact of selected thermal feedback effects

on the reactor performance and not to identify core configurations that meet specified design criteria (whose specification would again necessitate a clearer definition of mission requirements).

### III.A. Neutronic Modeling

The three-dimensional (3-D) continuous energy Monte Carlo code MCNP was used[25] for the neutronic modeling of the PBR. The MCNP code models a 3-D object by means of geometry cells defined by user-specified surfaces. The code can be used to calculate surface current, surface flux, track length estimate of cell flux, flux at a point (point detector), track length estimate of energy deposition, and track length estimate of fission energy deposition.

System description for MCNP modeling requires the following:

1. representing all surfaces by identification numbers and defining each of these surfaces by a set of equations
2. defining the cells, represented by identification numbers in terms of the union and intersection of surfaces
3. associating each cell with a specific material composition and temperature.

Since the PBR core has $\frac{1}{12}$ symmetry (see Fig. 4), a $\frac{1}{12}$ core with reflecting neutron surfaces along the symmetry planes was chosen to reduce the MCNP run time. The validity of this approach has been verified against whole-core MCNP calculations.[17] Figures 5, 6, and 7 show the MCNP modeling of the core, top reflector and bottom reflector, respectively. The numbers in Figs. 5, 6, and 7 denote the computational cells specified as input for MCNP. For example, cells 1, 10, 15, and 20 shown in Figs. 5 and 7 correspond to the hot gas ducts at the center of the fuel elements (i.e, outer plenum in Fig. 3). Cells 31, 34, 37, and 40 of Fig. 6 show that these ducts are plugged with graphite plugs at the inlet plenum to assure correct direction of gas flow. Table III gives the material densities for each cell defined in Figs. 5, 6, and 7. These material densities assume the following:

1. a reactor pressure of 60 atm
2. 50% porous frit material
3. 5% of core volume for $ZrH_{1.7}$ canning material.

Since the system under consideration uses highly enriched uranium (i.e., 93.5 wt% $^{235}U$ from Table II), the temperature feedback due to Doppler broadening of $^{238}U$ resonances in the slowing-down region is negligible. In that respect, the most important temperature effects occur during the process of neutrons achieving thermal equilibrium with the medium nuclei. The MCNP code models such temperature effects through both the free gas and $S(\alpha,\beta)$ models.[26] The $S(\alpha,\beta)$

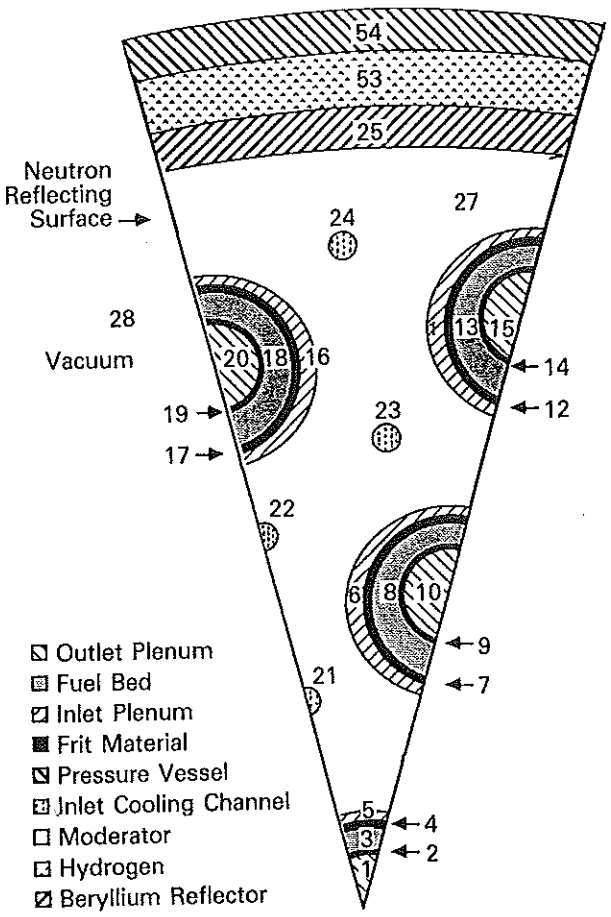


Fig. 5. One-twelfth radial section of PBR core.

model accounts for the lattice effects in describing scattering from bound nuclei and for the interference effects arising from the wave behavior of neutrons at low energies. The MCNP code uses the free-gas model down to an energy (or temperature) where $S(\alpha,\beta)$ data are available. At that point $S(\alpha,\beta)$ treatment automatically overrides the free-gas treatment. While the lattice effects are important for $ZrH_{1.7}$, and $S(\alpha,\beta)$ data up to 1200 K are available in the MCNP libraries, the $S(\alpha,\beta)$ temperature was specified to be 300 K for the implementations in Sec. IV for the following reasons:

1. Other hydride moderators have been proposed for PBRs (e.g., $Li^7H$) with different lattice effects. This study considers $ZrH_{1.7}$ as an example hydride moderator and in that respect tries to minimize the lattice specific effects on the results.

2. The temperature values in a substantial portion of the core at full power are expected to be higher than 1000 K (see Sec. IV.A). Hydrides tend to lose hydrogen above 600 K (Ref. 25) and the $S(\alpha,\beta)$ model approaches the free-gas model at such high temperatures.[26]

In all the MCNP runs, 4000 neutron histories were followed per criticality cycle and the results of 20 to

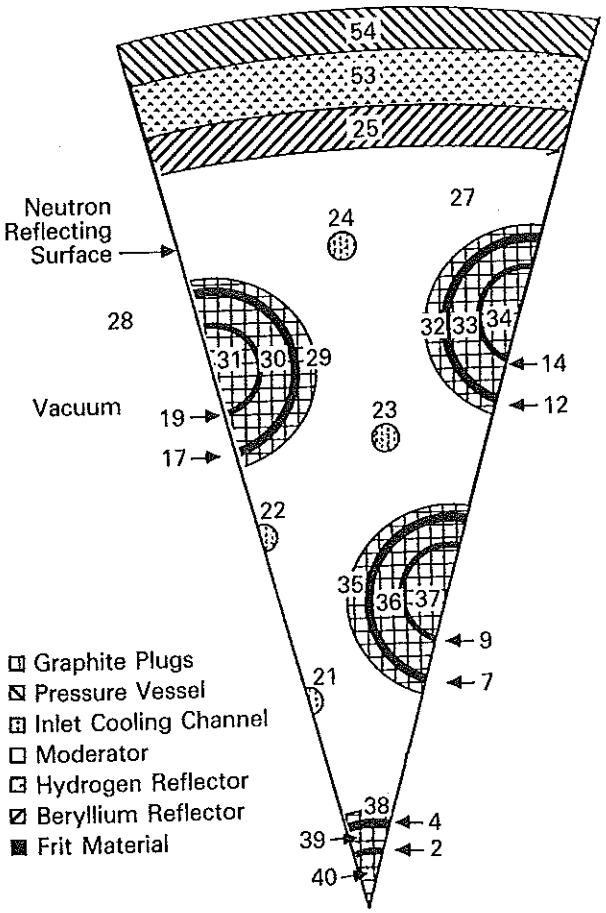


Fig. 6. One-twelfth radial section of PBR top reflector.

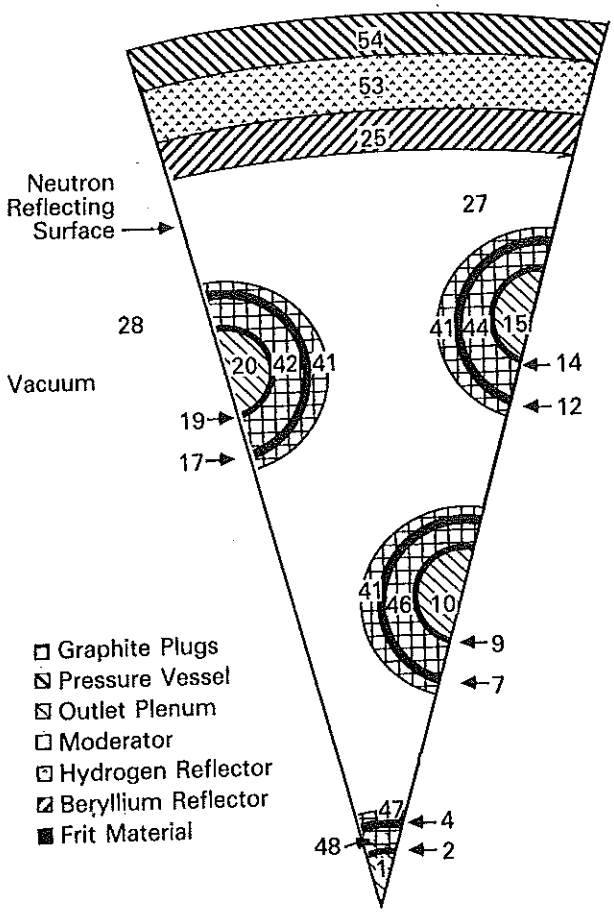


Fig. 7. One-twelfth radial section of PBR bottom reflector.

30 cycles were averaged to obtain good statistics (i.e., <0.005 deviation on $k_{eff}$).

### III.B. Thermal-Hydraulic Modeling

For the thermal-hydraulic modeling of the core, the core was assumed to be a homogeneous, porous medium with core porosity defined as the ratio of the material volume in the core to the total core volume. For a given power distribution, the temperature distribution in the core was found from the solution of[27,28]

$$\frac{1}{r}\frac{\partial}{\partial r}\left[r\frac{\partial T_s(r,z)}{\partial r}\right]+\frac{\partial^2 T_s(r,z)}{\partial z^2}+\frac{1}{k_{c,eff}}\left\{\dot{q}(r,z)-\epsilon h\frac{A_p}{V_p}[T_s(r,z)-T_f(z)]\right\}=0 \quad (1)$$

and

$$\frac{d^2T_f(z)}{dz^2}+\epsilon\frac{h}{k_f}\frac{A_p}{V_p}[T_{s,av}(z)-T_f(z)]=\frac{c_f\dot{m}}{\pi R^2 k_f}\frac{dT_f(z)}{dz}\ , \quad (2)$$

with

$$\left(\frac{\partial T_s}{\partial z}\right)_{z=L}=\left(\frac{\partial T_f}{\partial z}\right)_{z=L}=0\ , \quad (3)$$

$$T_s(r,0)=T_f(0)=T_i+\frac{Q_A}{\dot{m}c_f}\ , \quad (4)$$

$$\left(\frac{\partial T_s}{\partial r}\right)_{r=R}=-\frac{Q_A}{2\pi RLk_{c,eff}}\ , \quad (5)$$

$$\left(\frac{\partial T_s}{\partial r}\right)_{r=0}=0\ , \quad (6)$$

where

$$T_{s,av}(z)=\frac{2}{R^2}\int_0^R dr\, rT_s(r,z) \quad (7)$$

$r, z$ = distances from the core center and inlet, respectively

$R, L$ = core radius and height, respectively

$k_{c,eff}, \epsilon$ = effective core thermal conductivity and porosity, respectively

TABLE III

MCNP Cell Material Densities (Core Loading 8 kg $^{235}U$)

| Cell Name | Cell Number | Material | Density (atom/b·cm) |
|---|---|---|---|
| Outer plenum | 1, 10, 15, 20 | Hydrogen | $1.76 \times 10^{-3}$ |
| Hot frit | 2, 9, 14, 19 | ZrC (50% porous, hydrogen in free volume) | Zr: 0.01983<br>C: 0.01983<br>H: $8.84 \times 10^{-4}$ |
| Cold frit | 4, 7, 12, 17 | Zircaloy-2 (50% porous, hydrogen in free volume) | Zr: $2.126 \times 10^{-2}$ Cr: $2.163 \times 10^{-5}$<br>Sn: $3.13 \times 10^{-4}$ Ni: $9.733 \times 10^{-6}$<br>Fe: $2.92 \times 10^{-5}$ H: $8.840 \times 10^{-4}$ |
| Fuel bed | 3, 8, 13, 18 | UC kernel, ZrC coating (50% porous, hydrogen in free volume) | $^{235}U$: $1.077 \times 10^{-3}$ Zr: 0.02281<br>$^{238}U$: $7.396 \times 10^{-5}$ $^{12}C$: 0.02369<br>H: $6.94 \times 10^{-4}$ |
| Inlet plenum | 5, 6, 11, 16 | Hydrogen | $1.76 \times 10^{-3}$ |
| Inlet cooling channel | 21, 22, 23, 24 | Hydrogen | $1.76 \times 10^{-3}$ |
| Moderator | 27 | $ZrH_{1.7}$ | Zr: $3.564 \times 10^{-2}$ Cr: $3.170 \times 10^{-4}$<br>H: $6.058 \times 10^{-2}$ Ni: $2.33 \times 10^{-4}$<br>Fe: $1.213 \times 10^{-3}$ Mn: $3.730 \times 10^{-5}$ |
| Pressure vessel | 54 | Beryllium | 0.1238 |
| | | Stainless steel | Fe: $5.651 \times 10^{-2}$ Ni: $1.086 \times 10^{-2}$<br>Cr: $1.477 \times 10^{-2}$ Mn: $1.738 \times 10^{-3}$ |
| End reflectors | 29–48 | Carbon | 0.08032 |
| Annulus | 53 | Hydrogen | Variable |
| Radial reflector | 25 | Beryllium | 0.1238 |

$k_f, c_f, \dot{m}$ = hydrogen thermal conductivity, specific heat under constant pressure, and mass flow rate, respectively

$A_p, V_p$ = fuel particle surface area and volume, respectively

$Q_A$ = heat transfer rate into the annulus

$\dot{q}(r,z)$ = core power density at point $(r,z)$

$T_s(r,z)$ = core temperature at point $(r,z)$

$T_i$ = hydrogen temperature at the annulus inlet (at $z = L$ or $z' = 0$ in Fig. 1)

$T_f(z)$ = hydrogen temperature at distance $z$ from the core inlet (at $z = 0$ or $z' = L$ in Fig. 1)

$h$ = fuel pellet-to-coolant heat transfer coefficient.

In addition to the assumption of a homogeneous, porous core, Eqs. (1) through (6) assume the following:

1. radially uniform hydrogen temperature in the core
2. constant $k_{c,eff}$, $k_f$, and $c_f$
3. axially uniform heat transfer from the core into the annulus [Eq. (5)]
4. no heat loss from the hydrogen flowing through the annulus [Eq. (4)]
5. no axial heat transfer at the core exit [Eq. (3)].

Assumptions 1, 2, and 5 are based on preliminary parametric investigations using uniform core coolant temperatures between 300 and 1000 K, which showed that:

1. The value $T_s(r,z)$ is not too sensitive to the temperature dependence of either $k_{c,eff}$ or $c_f$.

2. Both the radial variation of $T_s(r,z)$ for a given $z$ (maximum 20 to 30 K) and also its axial variation near the exit (~20 K/cm) are small.

3. The difference between $T_{s,av}(z)$ and $T_f(z)$ for a given $z$ is small (a maximum of ~100 K near the center of the core).

Assumption 4 leads to the overestimation of temperature feedback from the hydrogen density changes in the annulus. Assumption 2 is also consistent with the

assumption of a homogeneous, porous core. Assumption 3 affects mainly the boundary condition given by Eq. (5) and will be justified in Sec. IV.A. For these preliminary parametric investigations and also for the analyses described in Sec. IV, the heat transfer coefficient in Eqs. (1) and (2) as stated in Ref. 28 is

$$h = 1.064 c_p G \left(\frac{c_p \dot{m}}{k_f}\right) \left(\frac{d_p G}{\dot{m}}\right)^{-0.041} , \qquad (8)$$

where

$c_p$ = specific heat of the fuel particle (J/kg·K)

$G$ = mass velocity (kg/m·s)

$d_p$ = particle diameter.

Other variables are as defined before with $\dot{m}$ in kg/s, $k_f$ in W/m·K, and $h$ in W/m$^2$·K.

For a given $\dot{q}(r,z)$ and $T_f(z)$, Eq. (1) was solved by the HEATING-5 code,[29] which is a generalized finite difference heat conduction code designed to solve steady-state and/or transient heat conduction problems in one-, two-, or three-dimensional Cartesian or cylindrical coordinates or one-dimensional spherical coordinates. Since $Q_A$ in Eqs. (4) and (5) is an unknown quantity, the following iterative procedure (inner iterations) was used for the solution of Eqs. (1) through (6):

1. Assume uniform $T_s(z)$.

2. Choose a $Q_A$ that is less than the total heat generated in the core since part of the generated heat is taken up by the hydrogen flowing through the annulus. The total heat generated in core is given by

$$2\pi \int_0^R r\,dr \int_0^L dz\,\dot{q}(r,z) .$$

3. Find $T_f(z)$ from Eqs. (2), with boundary conditions given by Eqs. (3) and (4).

4. Find $T_s(r,z)$ from the numerical solution of Eq. (1) using HEATING-5 with boundary conditions as given by Eqs. (3) through (6).

5. If

$$\text{abs}\left[2\pi R k_{c,eff} \int_0^L dz \left(\frac{\partial T_s}{\partial r}\right)_{r=R} + Q_A\right] < \delta ,$$

where $\delta$ is some specified small number, then STOP. Else GOTO step 2.

For the solution of Eq. (1) with the HEATING-5 code, each fuel element (Fig. 3) was divided into 10 parts axially to obtain the 10 pie-shaped volumes (see Fig. 8) and each pie-shaped volume was further divided into eight rings $r_i \le r \le r_{i+1}$ ($i = 0,\ldots,7$; $r_0 = 0$), which led to the partitioning of the core into 80 control volumes. The fission energy deposition rate in each of these control volumes was obtained from MCNP simulations and was assumed to be uniformly generated

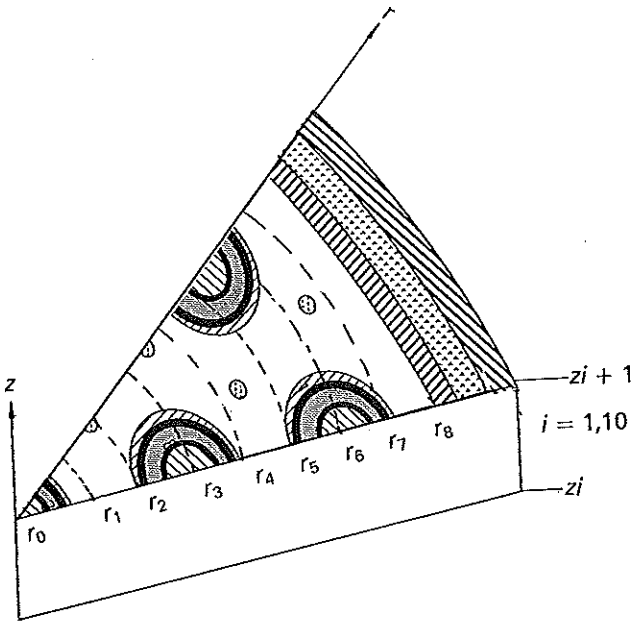


Fig. 8. Axial and radial partitioning of PBR core for HEATING-5 modeling.

within the control volume. Then the power $p_i$ ($i = 1, \ldots, 80$) generated in control volume $i$ was found from

$$p_i = \frac{\tilde{p}_i m_i}{\sum_{j=1}^{80} \tilde{p}_j m_j} P , \qquad (9)$$

where

$\tilde{p}_i$ = MCNP result for the energy deposited in control volume $i$ [in MeV/g(fuel)·n$^{-1}$]

$m_i$ = mass of fuel in the control volume $i$ (in grams)

$P$ = total reactor power (in megawatts).

To find $T_{s,av}(z)$ for the determination of $T_f(z)$ from Eq. (2), the $T_s(r,z)$ obtained from each HEATING-5 run were averaged over the pie-shaped volumes shown in Fig. 8 using Eq. (7), and the results of the averaging process were fitted to a second-order polynomial in $z$.

The two moderator materials considered in this study are beryllium and $ZrH_{1.7}$ (see Table I). The effective core conductivity (i.e., $k_{c,eff}$) in Eqs. (1) and (5) was assumed to be the conductivity of the pure moderator in view of the following considerations:

1. The core is being modeled as a homogeneous medium with uniform properties.

2. The governing equations [i.e., Eqs. (1) and (2)] do not account for radiative heat transfer. For systems with distributed heat sources at high temperatures (e.g., a waste canister containing spent-fuel rods at around

600°C), it has been shown that (a) radiative heat transfer can be a very important heat transfer mechanism,[30] and (b) pure radiative heat transfer leads to significantly higher temperatures in the system than both radiative and conductive heat transfer.[31] It has been also shown that this temperature increase in the system when the conduction mode is neglected becomes larger for temperatures expected to occur in the PBR fuel elements under operational conditions[31] (i.e., around 2000 to 2500 K). In that respect, using $k_m$ (which is larger in magnitude than $k_{c,eff}$) in Eqs. (1) and (5) leads to lower moderator temperatures and hence is a conservative assumption.

The conductivity for $ZrH_{1.7}$ was determined from[32]

$$k_m = 0.042 + 1.7910^{-5}T \ , \tag{10}$$

where $T$ is the temperature (in kelvins) and $k_m$ is the $ZrH_{1.7}$ conductivity (in calories per centimetre per second per kelvin). The variation in the hydrogen density with distance in the annulus was calculated from the $p$-$V$-$T$ relationship for compressible gases,[33] i.e.:

$$\rho(z') = \frac{p}{Z\bar{R}T(z')} \ , \tag{11}$$

with

$$T(z') = T_i + \frac{Q_A}{\dot{m}c_f}\frac{z'}{L} \tag{12}$$

where

$z'$ = axial distance from the entrance to the annulus (see Fig. 1)

$p$ = hydrogen pressure in the annulus (assumed to be uniform)

$Z$ = compressibility factor for hydrogen (averaged over the annulus)

$\bar{R}$ = 8.314 kJ/kmol·K = universal gas constant

$\rho(z'), T(z')$ = hydrogen density and temperature at $z'$, respectively.

Equation (12) also assumes that heat flux into the annulus is uniform and that there are no heat losses from the annulus. All the analyses were performed with $T_i$ = 100 K and $p$ = 60.8 bars (i.e., 60 atm). Table IV gives values of the PBR parameters fixed for the thermal-hydraulic analyses. Other PBR parameters used in the implementations in Sec. IV are given in Table II.

TABLE IV

PBR Parameters for Thermal-Hydraulic Modeling

| | |
|---|---|
| Pressure (atm) | 60 |
| Power (MW) | 150 |
| Core porosity | 0.4 |
| Hydrogen density (at 300 K and 60 atm) (kg/m$^3$) | 5.87 |
| Specific heat of hydrogen (300 K) (kJ/kg·K) | 14.31 |
| Fuel-to-hydrogen heat transfer coefficient [see Eq. (8)] (W/cm$^2$·K) | 18 720 |
| $ZrH_{1.7}$ conductivity (at 300 K) (W/m·K) | 2.28 |
| Beryllium conductivity (at 300 K) (W/m·K) | 200 |

TABLE V

Core Configurations Considered in the Implementations

(All other materials and dimensions are as given in Tables I and II.)

| Core Number | Core Loading (kg $^{235}$U) | Moderator Material | Reflector Thickness (cm) |
|---|---|---|---|
| 1 | 8 | $ZrH_{1.7}$ | 1 |
| 2 | 8 | $ZrH_{1.7}$ | 5 |
| 3 | 8 | $ZrH_{1.7}$ | 10 |
| 4 | 8 | Beryllium | 5 |
| 5 | 18 | Beryllium | 5 |

## IV. IMPLEMENTATION AND RESULTS

Table V lists the core configurations used for core and reflector analysis. As indicated in Sec. I, core analysis is directed toward investigation of the impact of the change in the core neutron spectrum due to the increased thermal motion of the fuel and moderator nuclei at operational conditions on $k_{eff}$, the steady-state core power, and temperature distributions. Reflector analysis investigates how a change in the fraction of neutrons reflected back to the core due to a change in the heat input into the annulus and/or hydrogen flow rate in the annulus affects these core characteristics. The $ZrH_{1.7}$ moderated cores in Table V have the optimum lattice pitch (taken from Ref. 17) that maximizes $k_{eff}$. The higher core loading of core 5 is achieved by using larger kernel size and a thinner outer coating without changing the overall fuel particle dimensions. Beryllium is chosen to be representative of the possible nonhydrogenous moderator materials (e.g., carbon, beryllium, BeO).

### IV.A. Core Analysis

Since initial runs of HEATING-5 using the inner iterations described in Sec. III.B showed that $Q_A$ in Eq. (5) is <1% of total reactor power, the boundary condition given by Eq. (5) was replaced by an adiabatic boundary condition at $R$ (which also justifies assumption 3 in Sec. III.B) to save computational time by avoiding these inner iterations in the implementations.

For the outer iterations, the power distribution obtained from MCNP [i.e., $q(r,z)$] was used as input for

the solution of Eq. (1) and the $T_s(r,z)$ obtained from the solution of the Eq. (1) with this $q(r,z)$ was used as input for the next MCNP run until the $k_{eff}$ and the $q(r,z)$ obtained from two successive sets of calculations agreed within the statistical error on the results. Table VI shows how $k_{eff}$ changes during these outer iterations for cores 2 and 3 (see Table V). One outer iteration is defined as the determination of one pair of $q(r,z)$, $T_s(r,z)$ distributions. Table VI shows that the iterations converge very rapidly and that the temperature effect on $k_{eff}$ is quite large (i.e., about 1.6% $\Delta k/k$ and 1.2% $\Delta k/k$ for cores 2 and 3, respectively).

The change in the axial distribution of local power/average power ratio due to temperature feedback in cores 2 and 3 is shown in Figs. 9 and 10, respectively. The vertical bars on the data points in Figs. 9 and 10 indicate the magnitude of the statistical uncertainty on the results due to the Monte Carlo approach used by the MCNP code. Local power is the power generated in each pie-shaped region shown in Fig. 8. Average power is the total power divided by the number of these regions (i.e., 10). The figures show that while there is some change in the axial power profile, the change is small. The maximum change in local power is 5% (at $z = 27$ cm in Fig. 9) and the maximum shift in the hot spot location is found to be ~3 cm for both cores. Figures 9 and 10 also show that most of the changes are within the statistical uncertainty on the results. The $T_{s,av}(z)$ corresponding to Figs. 9 and 10 are shown in Figs. 11 and 12, respectively, which indicate that core temperature distributions are not significantly affected by the neutronic/thermal-hydraulic coupling. The difference between the radially averaged core temperature $T_{s,av}(z)$ and the hydrogen temperature $T_f(z)$ is shown as a function of $z$ in Figs. 13 and 14 for cores 2 and 3, respectively. These figures show that the maximum temperature difference occurs near the center of the core and is ~100 K.

Since (a) the absorption cross section of hydrogen is orders of magnitude higher than that for other possible nonhydrogenous moderators (e.g., beryllium, BeO, carbon) and also varies fairly rapidly in the electron-volt energy range, and (b) $^{235}U$ has resonances in the electron-volt to kilo-electron-volt range, another set of coupled neutronic/thermal-hydraulic analyses were performed with two beryllium-moderated cores (i.e., cores 4 and 5 in Table V) to investigate whether the temperature effects on $k_{eff}$ were arising from change in the

TABLE VI

Variation of $k_{eff}$ During Outer Iterations for Core Analysis: Cores 2 and 3 (see Table V)

| Core Number | Iteration Number | $k_{eff}$ (% deviation) |
|---|---|---|
| 2 | 1 | 0.988 (0.35) |
| | 2 | 0.972 (0.38) |
| | 3 | 0.972 (0.46) |
| 3 | 1 | 1.014 (0.36) |
| | 2 | 1.008 (0.41) |
| | 3 | 1.002 (0.56) |
| | 4 | 1.002 (0.41) |

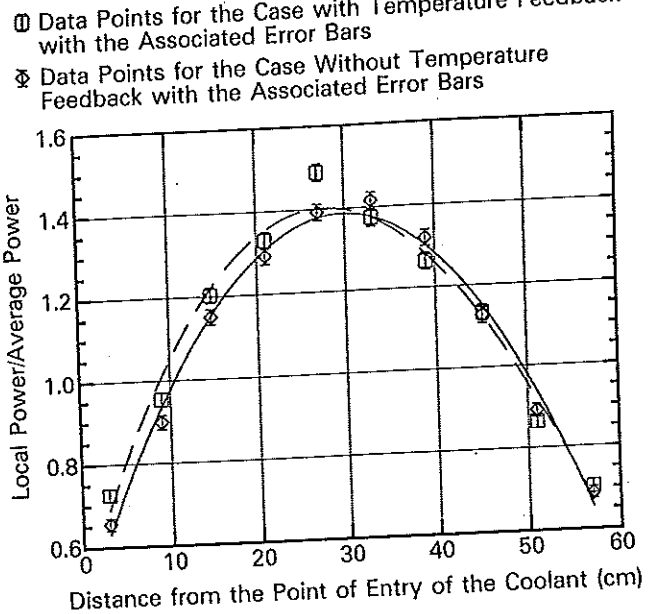


Fig. 9. Axial distribution of the local power/average power ratio in core 2.

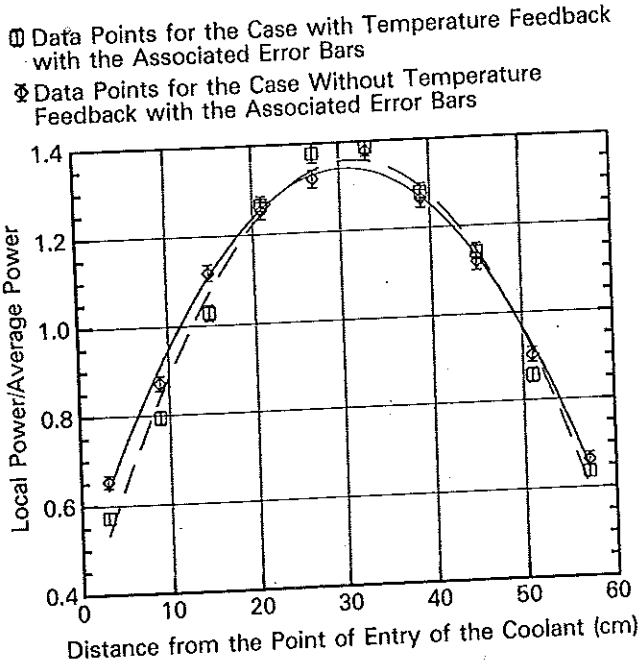


Fig. 10. Axial distribution of the local power/average power ratio in core 3.

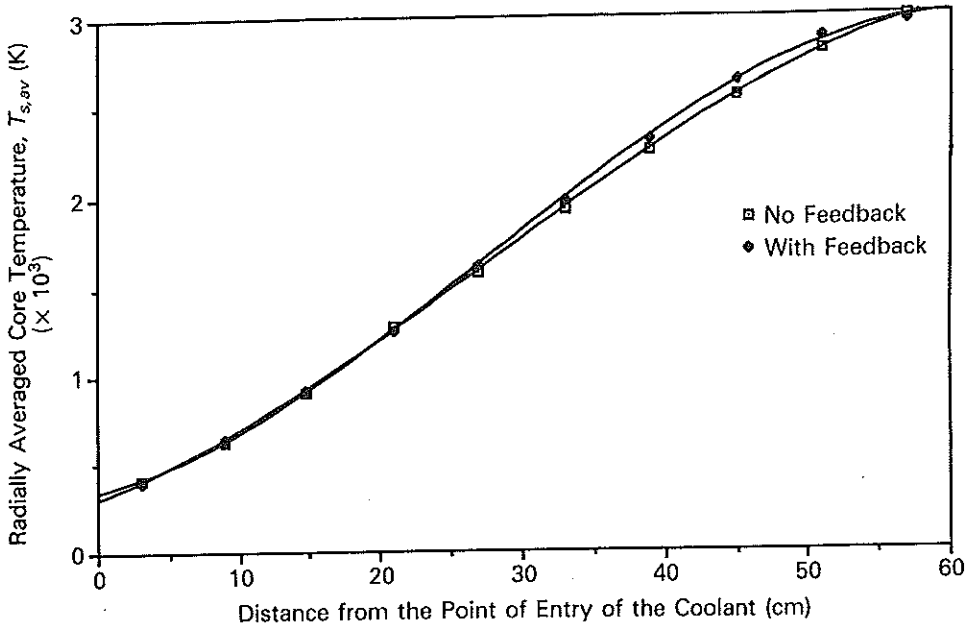


Fig. 11. Radially averaged core temperature as a function of distance from the point of entry of the coolant for core 2.

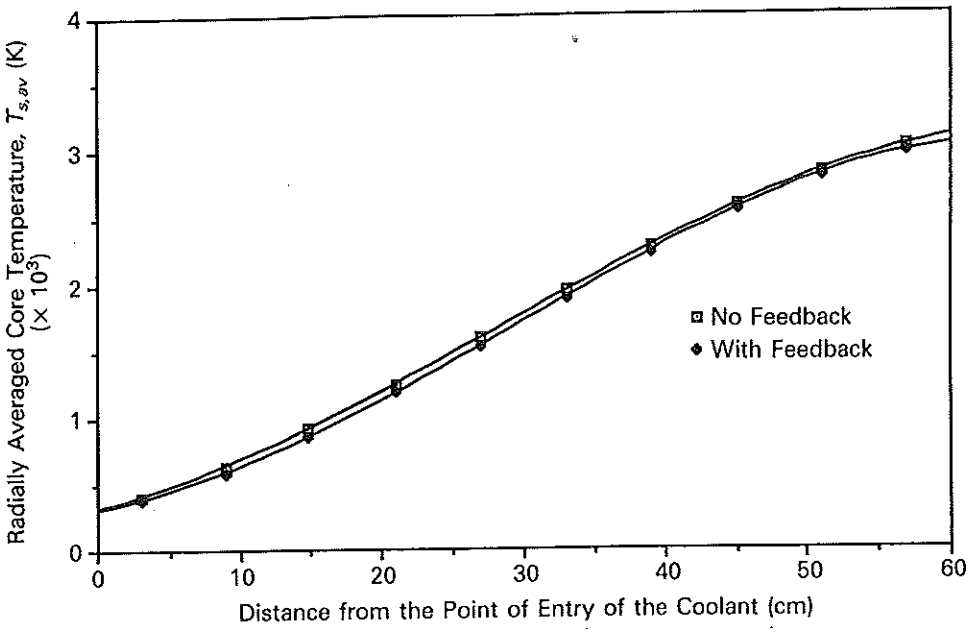


Fig. 12. Radially averaged core temperature as a function of distance from the point of entry of the coolant for core 3.

absorption rate in hydrogen or the fission rate with temperature. Table VII shows the variation of $k_{eff}$ with temperature feedback in cores 4 and 5, and Figs. 15 and 16 show the corresponding changes in the axial distribution of local power/average power ratio. Table VII and Figs. 15 and 16 indicate that the temperature effects due to spectral shift are smaller in cores 4 and 5, with virtually no change in the power distribution (which is why error bars reflecting the statistical uncertainty in MCNP results are not shown in Figs. 15 and 16). Hence, the change in the absorption rate in hydrogen seems to be the major contributor to the temperature effects observed in cores 2 and 3 and subsequently PBRs using hydrogenous moderators are expected to be more strongly affected by the temperature effects than those using nonhydrogenous moderators.

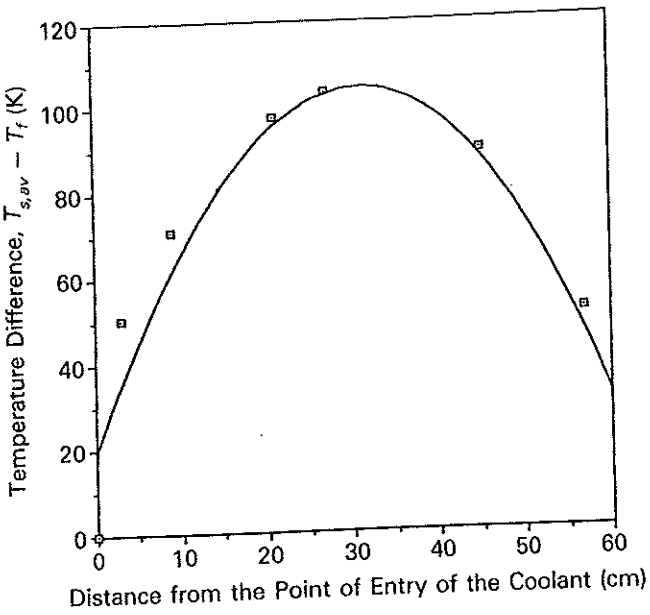


Fig. 13. Temperature difference between the solid and the coolant in core 2.

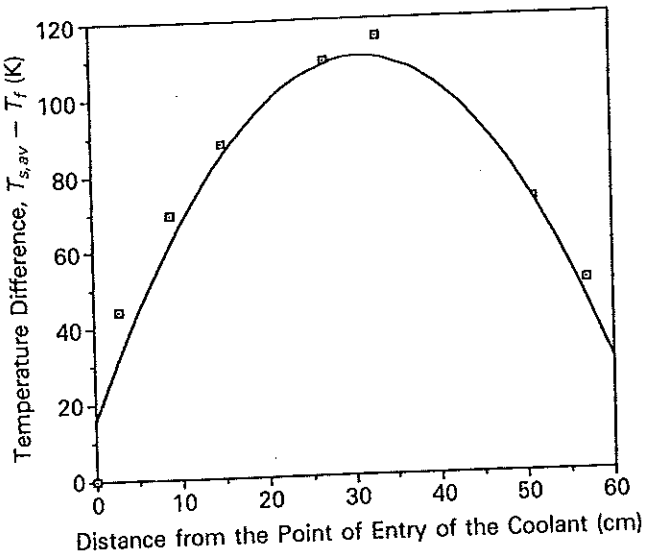


Fig. 14. Temperature difference between the solid and the coolant in core 3.

TABLE VII

Variation of $k_{eff}$ During Outer Iterations for Core Analysis: Cores 4 and 5 (see Table V)

| Core Number | Iteration Number | $k_{eff}$ (% deviation) |
|---|---|---|
| 4 | 1 | 0.826 (0.50) |
| | 2 | 0.820 (0.43) |
| | 3 | 0.820 (0.39) |
| 5 | 1 | 0.749 (0.43) |
| | 2 | 0.741 (0.38) |
| | 3 | 0.741 (0.45) |

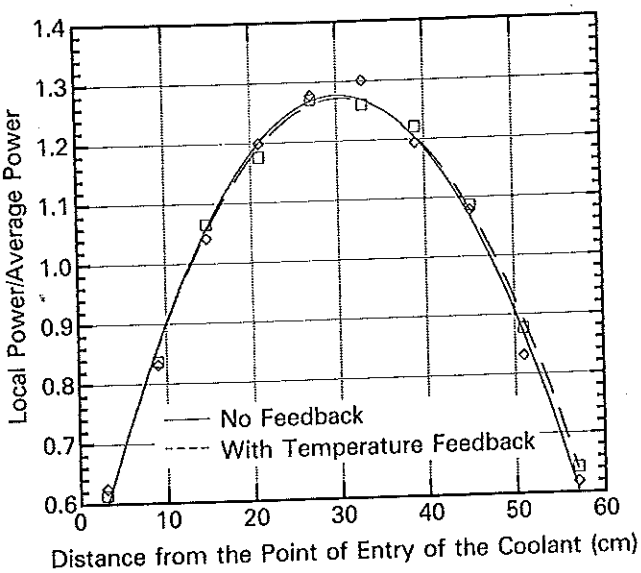


Fig. 15. Axial distribution of the local power/average power ratio in core 4.

### IV.B. Reflector Analysis

While a change in the hydrogen temperature distribution in the annulus, in principle, affects $Q_A$ in Eq. (5) and hence the core power distribution, Sec. IV.A shows that $Q_A$ is a very small fraction of the total core power and furthermore core power distribution is relatively insensitive to temperature feedback. In that respect, neither inner nor outer iterations needed to be used in reflector analysis and reflector analysis consisted of investigating only the variation of the $k_{eff}$ for cores 1, 2, and 3 (see Table V) as a function of annulus gap width and hydrogen mass flow rate in the annulus [or rather $Q_A/\dot{m}$ ratio in Eq. (4)], accounting for both the spectrum and density effects. As indicated in Sec. I, an earlier study that used a beryllium-moderated PBR with uniform hydrogen temperatures in the annulus indicates that the temperature of the hydrogen in the annulus may affect $k_{eff}$ appreciably.[17]

For reflector analysis, the annulus was axially divided into 10 regions in a manner similar to the axial partitioning of the core (see Sec. III.B). The hydrogen temperature and density in each region were determined from Eqs. (11) and (12), respectively, using a $z'$ that corresponded to the midpoint of the region. The results are shown in Table VIII. The following observations are made from Table VIII:

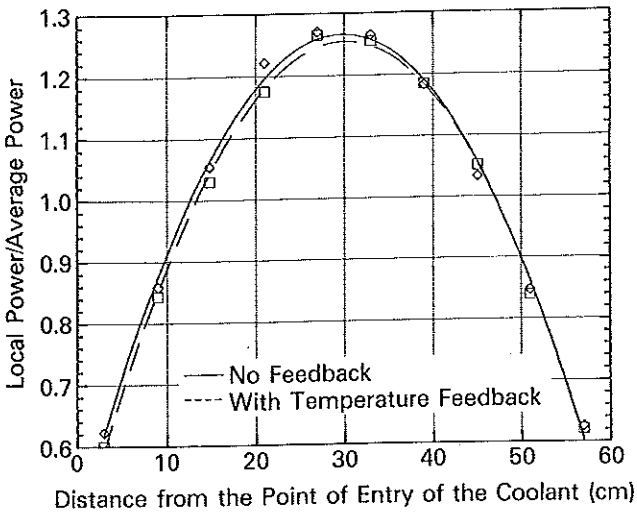


Fig. 16. Axial distribution of the local power/average power ratio in core 5.

1. The $k_{eff}$ of all the cores with a 5-cm annulus gap size slightly increases with an increasing $Q_A/\dot{m}$ ratio.

2. When the gap size is 10 cm, the $k_{eff}$ for cores 1, 2, and 3 exhibits no change, a slight decrease, and a slight increase, respectively, with an increasing $Q_A/\dot{m}$ ratio.

3. The $k_{eff}$ decreases substantially in core 1 with increasing annulus gap size both for high and low $Q_A/\dot{m}$ ratios.

4. For cores 2 and 3, $k_{eff}$ does not change with increasing annulus gap size for the low $Q_A/\dot{m}$ ratio, but a rather large decrease occurs in core 2 for the high $Q_A/\dot{m}$ case.

5. The $k_{eff}$ slightly increases with increasing annulus gap size for the high $Q_A/\dot{m}$ ratio in core 3.

Observations 1 and 3 imply that the hydrogen in the annulus behaves as an absorber rather than a reflector for cores 1, 2, and 3. This implication was further verified by two additional MCNP runs where the hydrogen in the annulus was uniformly maintained at 100 and at 500 K. It was noted that the $k_{eff}$ is greater when the temperature of hydrogen in the annulus is higher. Observations 1 and 2 and the statistical uncertainties on the results imply that, for fixed annulus gap size, $k_{eff}$ for cores 1, 2, and 3 is not very sensitive to the $Q_A/\dot{m}$ ratio. The low and high $Q_A/\dot{m}$ ratios considered in the study (i.e., 625 and 15 000 kJ/kg, respectively) correspond to annulus inlet-to-outlet hydrogen density ratios of 1.44 and 11.5, respectively, and hence cover a broad hydrogen density range. This result is interesting because a finding of Ref. 17, which uses two very similar PBRs moderated with beryllium instead of $ZrH_{1.7}$ and with 30- and 45-cm core diameters (instead of the 22.5 cm used in this study as shown in Table II), is that while a hydrogen density change in the annulus corresponding to a uniform temperature change from 100 to 500 K (also at 60 atm) leads to a 1.1% $\Delta k/k$ decrease in the $k_{eff}$ of the smaller core, the decrease observed in the $k_{eff}$ of the larger core is also very small (0.2% $\Delta k/k$).

TABLE VIII

Variation of $k_{eff}$ with Annulus Gap Size and $Q_A/\dot{m}$ Ratio for Cores 1, 2, and 3 (see Table V)

| Annulus Gap Size (cm) | $k_{eff}$ (% deviation) for $Q_A/\dot{m}$ = 625 kJ/kg / $k_{eff}$ (% deviation) for $Q_A/\dot{m}$ = 15 000 kJ/kg | | |
|---|---|---|---|
| | Core 1 | Core 2 | Core 3 |
| 5.0 | 0.942 (0.53) / 0.948 (0.43) | 0.988 (0.36) / 0.994 (0.53) | 1.015 (0.42) / 1.017 (0.46) |
| 10.0 | 0.930 (0.46) / 0.930 (0.36) | 0.988 (0.35) / 0.983 (0.40) | 1.015 (0.42) / 1.022 (0.45) |

A possible physical explanation for the $k_{eff}$ behavior reported in Ref. 17 and the implications of observations 1, 2, and 3 can be given in terms of the spectrum of the neutrons entering the annulus. The small beryllium-moderated core used in Ref. 17 has a lower moderator-to-fuel ratio and the neutrons entering the annulus have a harder spectrum. Hence scattering events dominate in the hydrogen and reflection from the hydrogen and from the stainless steel pressure vessel contributes to neutron economy. For the large beryllium-moderated core of Ref. 17, neutrons entering the annulus have a softer spectrum due to the increased moderator-to-fuel ratio. Since hydrogen is a $1/v$ absorber, there are fewer neutrons reflected back from the hydrogen and stainless steel pressure vessel in this case and hence a smaller decrease in $k_{eff}$ results due to hydrogen density change caused by the temperature change. For the $ZrH_{1.7}$ core used in this study, the lattice pitch maximizes $k_{eff}$ as indicated before, and the neutrons entering the annulus have an even softer spectrum, which leads to hydrogen acting as an absorber. Although density of the hydrogen in the annulus decreases with an increasing $Q_A/\dot{m}$ ratio, absorption in the hydrogen is still strong enough that there is no appreciable change in the number of neutrons reaching the pressure vessel and subsequently the number of neutrons reflected back. However, while these arguments explain why the hydrogen in the annulus acts as an absorber and why $k_{eff}$ is not sensitive to the $Q_A/\dot{m}$ ratio for fixed annulus gap size, observations 3, 4, and 5 could not be explained in a consistent manner using similar simple physical arguments. These observations are attributed to a complex energy-space-angle-temperature relationship in neutron transport between the beryllium reflector, annulus, and pressure vessel, and possibly the core.

## V. CONCLUSION

This study uses $ZrH_{1.7}$ and beryllium-moderated PBRs to investigate the impact of neutronic/thermal-hydraulic coupling in the design and performance assessment of solid core, thermal reactors for NTP. The results of this study show the following:

1. Substantial reduction in $k_{eff}$ may occur for reactors using hydrogenous moderators in going from cold to operational temperatures, and hence, a realistic estimation of fuel, core size, and control requirements necessitate coupled neutronic/thermal-hydraulic studies for reactors using such moderators.

2. Due to the possible additional tight energy-space-angle-temperature coupling in neutron transport between the reflector, annulus, and pressure vessel, optimization of the engine design is also expected to require fully integrated studies. For example, hydrogen flow rate in the annulus may influence the optimum reflector thickness and annulus gap size (see observation 4 in Sec. V.B).

3. Since no appreciable distortion was observed with temperature feedback in the axial power profile of both the $ZrH_{1.7}$ and beryllium-moderated PBRs, it may be possible to estimate the thermal safety margins and propellant exit temperatures based on power distributions obtained from neutronic calculations at room temperature.

4. While variation of the hydrogen flow rate in the annulus has been proposed as a partial control mechanism, such a control mechanism may not be feasible for reactors with high moderator-to-fuel ratios (and hence soft core spectra). In fact, for such reactors $k_{eff}$ is expected to increase with decreasing hydrogen density in the annulus, and it may be difficult to mitigate the consequences of a loss of pressure accident in the annulus.

The study also shows that the radial temperature distribution in solid core material and the coolant/propellant is fairly uniform (within 20 to 30 K), and the maximum temperature difference between the solid and the coolant is small (~100 K near the center of the core), as expected from the large heat transfer area in fuel. It should be indicated, however, that the impact of temperature feedback on power distribution would be more pronounced in practice than those predicted by this study in view of the conservative assumptions made in the study (i.e., no Doppler, thermal expansion, or lattice effects; no radiative heat transfer). For example, core dimensional changes due to thermal expansion could impact both $k_{eff}$ and the power distribution by changing the amount of neutrons streaming through the annulus. Similarly, as indicated in Sec. III.B, radiative heat transfer can be a very important heat transfer mechanism for the PBR, and it has been shown[30] that pure radiative heat transfer leads to significantly higher temperatures in the system than both radiative and conductive heat transfer. In these respects, further work is needed to generalize the results given here.

## REFERENCES

1. L. N. MYRABO and J. R. POWELL, "Nuclear Reactor Sources for Space Prime Propulsion and Power," *Orbit-Raising and Maneuvering Propulsion: Research Status and Needs,* L. H. CAVENY, Ed., *Progress in Astronautics and Aeronautics*, **89**, 405, American Institute of Aeronautics and Astronautics, New York (1983).

2. P. W. GARRISON, K. T. NOCK, and R. JONES, "Nuclear Electric Propulsion (NEP) Spacecraft Configuration Study," *Orbit-Raising and Maneuvering Propulsion: Research Status and Needs*, L. H. CAVENY, Ed., *Progress in Astronautics and Aeronautics*, **89**, 544, American Institute of Aeronautics and Astronautics, New York (1983).

3. J. R. POWELL and T. E. BOTTS, "Particle Bed Reactors for Space Power and Propulsion," *Orbit-Raising and Maneuvering Propulsion: Research Status and Needs*, L. H. CAVENY, Ed., *Progress in Astronautics and Aeronautics*, **89**, 495, American Institute of Aeronautics and Astronautics, New York (1983).

4. H. J. SNYDER and T. A. SGAMMATO, "STAR-C Space Nuclear Power Application Studies," *Proc. 25th Intersociety Energy Conversion Engineering Conf.*, IECEC-90, P. A. NELSON, W. W. SCHERTZ, and R. H. TILL, Eds., p. 135, American Institute of Chemical Engineers, New York (1990).

5. M. M. PANICKER and E. T. DUGAN, "Static and Dynamic Neutronic Analysis of a Bimodal Gaseous Core Reactor System for Space Power," *Proc. 25th Intersociety Energy Conversion Engineering Conf.*, IECEC-90, P. A. NELSON, W. W. SCHERTZ, and R. H. TILL, Eds., p. 150, American Institute of Chemical Engineers, New York (1990).

6. J. MALLOY and D. POTEKHEN, "A Conceptual Study of the Use of a Particle Bed Reactor Nuclear Propulsion Model for the Orbital Maneuvering Vehicle," *Proc. 24th Intersociety Energy Conversion Engineering Conf.*, IECEC-89, W. D. JACKSON, Ed., p. 1209, Institute of Electrical and Electronics Engineers, New York (1989).

7. E. BAUMEISTER, R. ROVANG, J. MILLS, J. SERCEL, and R. FRISBEE, "A Potassium Rankine Multimegawatt Nuclear Electric Propulsion Concept," *Proc. 25th Intersociety Energy Conversion Engineering Conf.*, IECEC-90, P. A. NELSON, W. W. SCHERTZ, and R. H. TILL, Eds., p. 121, American Institute of Chemical Engineers, New York (1990).

8. D. DAROOKA, "A Comparison of Alternative Propulsion Systems for Lunar Cargo Transport," *AIAA/NASA/OAI Conf. Advanced SEI Technologies*, Cleveland, Ohio,

September 3-6, 1991, Paper #91-3563, available from the AIAA Library, AIAA Technical Information Service, 555 W. 57th, Suite 1200, New York 10019.

9. D. PELACCIO, C. SCHELL and J. LIVINGSTON, "Updated Solid-Core Nuclear Thermal Propulsion Engine Trades," *AIAA/NASA/OAI Conf. Advanced SEI Technologies*, Cleveland, Ohio, September 3-6, 1991, Paper #91-3507, available from the AIAA Library, AIAA Technical Information Service, 555 W. 57th, Suite 1200, New York 10019.

10. H. W. BRANDHORST and R. J. SOVIE, "Nuclear Technology and Space Exploration Missions," *Proc. 25th Intersociety Energy Conversion Engineering Conf.*, IECEC-90, P. A. NELSON, W. W. SCHERTZ, and R. H. TILL, Eds., p. 84, American Institute of Chemical Engineers, New York (1990).

11. J. S. CLARK, T. J. WICKENHEISER, A. MARSHALL, A. A. BHATTACHARYA, and J. WARREN, "NASA/DOE/DOD Nuclear Propulsion Technology Planning: Summary of FY 1991 Interagency Panel Results," NASA TM-102703, NASA Lewis Research Center (1992).

12. S. K. BOROWSKI, "Nuclear Thermal Rocket Workshop Reference System-ROVER/NERVA," *Nuclear Thermal Propulsion*, NASA CP-10079, p. 53, NASA Lewis Research Center (1991).

13. G. FARBMAN, "Upgraded NERVA Systems: ENABLER Nuclear System," *Nuclear Thermal Propulsion*, NASA CP-10079, p. 105, NASA Lewis Research Center (1991).

14. J. H. RAMSTHALER, "Low Pressure Nuclear Thermal Reactor Concept," *Nuclear Thermal Propulsion*, NASA CP-10079, p. 127, NASA Lewis Research Center (1991).

15. H. LUDEWIG, "Particle Bed Reactor Concept," *Nuclear Thermal Propulsion*, NASA CP-10079, p. 151, NASA Lewis Research Center (1991).

16. S. ANGHAIE, G. J. FELLER, S. D. PEERY, and R. C. PARSLEY, "Multigroup Calculation of Criticality and Power Distribution in a Two-Pass Fast Spectrum Cermet-Fueled Reactor," *Trans. Am. Nucl. Soc.*, **66**, 249 (1992).

17. T. HILSMEIER and T. ALDEMIR, "A Parametric Neutronic Study of a Nuclear Propulsion Engine Concept," *Advances in Mathematics, Computations and Reactor Physics*, 4.2(2.1-2.12), American Nuclear Society, La Grange Park, Illinois (1991).

18. T. A. HILSMEIER, S. M. AITHAL, and T. ALDEMIR, "How Useful Is Neutron Diffusion Theory for Nuclear Rocket Engine Design?" *Trans. Am. Nucl. Soc.*, **66**, 246 (1992).

19. A. C. KLEIN and B. R. LEWIS, "Design Tool Needs for Space Nuclear Propulsion Systems," *Trans. Am. Nucl. Soc.*, **66**, 257 (1992).

20. J. J. BUKSA, W. J. RIDER, M. HALL, R. T. PERRY, and M. HOUTS, "Integrated Analysis of Nuclear Thermal Rocket System Performance," *Trans. Am Nucl. Soc.*, **66**, 258 (1992).

21. D. DOBRANICH, "A Computer Program for Simulations of Space Reactor System Performance," *Trans. Am. Nucl. Soc.*, **66**, 259 (1992).

22. J. CLARK and T. MILLER, "The NASA/DOE/DOD Nuclear Rocket Propulsion Project," *AIAA/NASA/OAI Conf. Advanced SEI Technologies*, Cleveland, Ohio, September 3-6, 1991, Paper #91-3413, available from the AIAA Library, AIAA Technical Information Service, 555 W. 57th, Suite 1200, New York 10019.

23. M. SÖZEN, K. VAFAI, and L. A. KENNEDY, "Analysis of Thermal Charging and Discharging for Sensible Heat and Latent Heat Storage of Packed Beds," *AIAA J. Thermophys. Heat Transfer*, **5**, 623 (1991).

24. J. POWELL and F. HORN, "Direct Thrust Nuclear Propulsion Based on Particle Bed Reactors," Space Propulsion Workshop, AFRPL CP-85-002, Air Force Propulsion Laboratory, Edwards Air Force Base (1985).

25. J. S. BREIMEISTER, "MCNP—A General Monte Carlo Code for Neutron and Photon Transport, Version 3B," LA 7396-M, Los Alamos National Laboratory (1989).

26. G. I. BELL and S. GLASSTONE, *Nuclear Reactor Theory*, p. 337, Van Nostrand Reinhold, New York (1970).

27. M. SÖZEN and K. VAFAI, "Analysis of the Non-Thermal Equilibrium Condensing Flow of a Gas Through a Packed Bed," *Int. J. Heat Mass Transfer*, **33**, 1247 (1990).

28. K. VAFAI and M. SÖZEN, "Analysis of Energy and Momentum Transport for Fluid Flow Through a Porous Bed," *J. Heat Transfer*, **112**, 690 (1990).

29. W. D. TURNER, D. C. ELROD, and I. I. SIMANTOV, "HEATING-5—An IBM 360 Heat Conduction Program," ORNL/CSD/TM-15, Oak Ridge National Laboratory (1977).

30. K. VAFAI and J. ETTEFAGH, "Analysis of the Radiative and Conductive Heat Transfer Characteristics of a Waste Package Canister," *ASME J. Heat Transfer*, **110**, 1011 (1988).

31. K. VAFAI and J. ETTEFAGH, "The Effects of Stabilizers on the Heat Transfer Characteristics of a Nuclear Waste Canister," BMI/ONWI-612, Battelle Memorial Institute (1986).

32. R. SCHLICHT, Private Communication, GA Technologies, San Diego (Sep. 1992).

33. M. J. MORAN and H. N. SHAPIRO, *Fundamentals of Engineering Thermodynamics*, 2nd ed., p. 93, John Wiley & Sons, New York (1992).

**Shashikant M. Aithal** (BS, electrical engineering, University of Bombay, India, 1990; MS, nuclear engineering, The Ohio State University, 1993) is currently working toward a PhD in mechanical engineering at The Ohio State University. His current interests also include areas of plasma physics and its applications in space propulsion.

**Tunc Aldemir** (BS, mathematical physics, Istanbul University, Turkey, 1971; MS, 1975, and PhD, 1978, nuclear engineering, University of Illinois) is an associate professor of nuclear and mechanical engineering at The Ohio State University. He has 10 years of experience with small, compact core design/optimization and safety analysis and has served as an International Atomic Energy Agency expert in these areas. His current interests also include probabilistic risk assessment and reactor systems with passive safety features.

**Kambiz Vafai** (BS, mechanical engineering, University of Minnesota, 1975; MS, 1977, and PhD, 1980, mechanical engineering, University of California–Berkeley) is professor of mechanical engineering at The Ohio State University. He is a fellow of the American Society of Mechanical Engineers and recipient of the college of engineering Outstanding Research Award in both junior and senior faculty categories. He has more than 10 years of experience in the areas of transport through porous media and multiphase transport, natural convection in complex configurations, and high-energy storage and recovery processes.